Biometals (2012) 25:95–102
DOI 10.1007/s10534-011-9485-7

Inhibition of fumarase by bismuth(III): implications for the tricarboxylic acid cycle as a potential target of bismuth drugs in *Helicobacter pylori*

Zhuo Chen · Qinglu Zhou · Ruiguang Ge

Received: 19 July 2011 / Accepted: 27 July 2011 / Published online: 5 August 2011

Abstract *Helicobacter pylori* causes various gastric diseases, such as gastritis, peptic ulcerations and gastric cancer. Triple therapy combining bismuth compounds with two antibiotics is the cornerstone of the treatment of *H. pylori* infections. Up to now, the molecular mechanisms by which bismuth inhibits the growth of *H. pylori* are far from clear. In the bacterial tricarboxylic acid (TCA) cycle, fumarase catalyses the reversible hydration of fumarate to malic acid. Our previous proteomic work indicated that fumarase was capable of bismuth-binding. The interactions as well as the inhibitory effects of bismuth to fumarase have been characterized in this study. The titration of bismuth showed that each fumarase monomer binds one mol equiv of Bi^{3+}, with negligible secondary structural change. Bismuth-binding results in a near stoichiometric inactivation of the enzyme, leading to an apparent non-competitive mechanism as reflected by the Lineweaver–Burk plots. Our collective data indicate that the TCA cycle is a potential molecular target of bismuth drugs in *H. pylori*.

Keywords *Helicobacter pylori* · Fumarase · Bismuth · Tricarboxylic acid cycle

Abbreviations

DTNB	5,5′-Dithiobis(2-nitrobenzoic acid)
FRD	Fumarate reductase
H. pylori	*Helicobacter pylori*
FPLC	Fast protein liquid chromatography
MS	Mass spectrometer
PBS	Phosphate-buffered saline
SDH	Succinate dehydrogenase
SDS–PAGE	Sodium dodecyl sulfate–polyacrylamide gel electrophoresis
TCA	Tricarboxylic acid

Introduction

Helicobacter pylori is a Gram-negative bacterium causing various gastric diseases, including gastritis, peptic ulcerations, gastric carcinoma and mucosa-associated lymphoid tissue lymphoma (Blaser 1987). Bismuth compounds, such as colloidal bismuth subcitrate and ranitidine bismuth citrate, exhibit synergism with antibiotics against *H. pylori* and the triple therapy (bismuth/metronidazole/amoxicillin or tetracycline) is the cornerstone of the treatment of *H. pylori* infections (Xia et al. 2002). Although the acquisition of antibiotic resistance by *H. pylori* is the main cause of the treatment failure (Megraud 2004), primary or acquired resistance of *H. pylori* to bismuth

Zhuo Chen and Qinglu Zhou contribute equally to this work.

Z. Chen · Q. Zhou · R. Ge (✉)
The Laboratory of Integrative Biosciences,
College of Life Sciences, Sun Yat-Sen University,
Guangzhou 510275, China
e-mail: gerg@mail.sysu.edu.cn

compounds has not yet been reported. The molecular mechanisms by which bismuth inhibits the growth of *H. pylori* are far from clear, while all current hypotheses point to the binding of bismuth to the metal-binding sites in various metalloproteins (Ge and Sun 2007; Ge et al. 2007). Enzyme inhibition is supposed to play an important role in the action of bismuth-containing drugs, as the in vitro studies showed that Bi^{3+} can bind to the active sites of urease (Zhang et al. 2006) and alcohol dehydrogenase (Jin et al. 2004), resulting in the inhibition of the catalytic activities of these enzymes. Some other proposed target proteins are metallothioneins (Sun et al. 1999), the histidine-rich protein Hpn (Ge et al. 2006a, b), and serum proteins such as transferrin, lactoferrin and serum albumin (Sun and Szeto 2003).

The tricarboxylic acid (TCA) cycle is bifunctional in cell metabolism, providing biosynthetic precursors such as α-ketoglutarate, succinyl-CoA and oxaloacetate on one hand for a wide spectrum of cell components, while on the other hand acting as a metabolic energy source through the generation of reduced nucleotides whose re-oxidation may be coupled to ATP synthesis (Pitson et al. 1999). Despite the lack of the four key TCA cycle enzymes, i.e. α-ketoglutarate dehydrogenase, succinate dehydrogenase (SDH), succinyl-CoA synthetase and malate dehydrogenase based on genome-wide prediction (Tomb et al. 1997), the activities of all these relevant enzymes were observed in *H. pylori* (Ge 2002). During the TCA cycle, fumarate reductase (FRD) catalyses the unidirectional conversion of fumarate to succinate with the reverse reaction catalysed by SDH. FRD is essential for *H. pylori* colonization in the mouse stomach (Ge et al. 2000) and was a potential therapeutic target (Mendz et al. 1995; Ge 2002). In the TCA cycle, fumarase catalyses the reversible hydration of fumarate to malic acid. The mutation of fumarase is known to be related to the highly metastatic and unusually lethal hereditary leiomyomatosis renal cell carcinoma (Sudarshan et al. 2007; Yang et al. 2010). Our previous proteomic work indicated that fumarase was capable of bismuth-binding and was one of the principal targeting sites in vivo (Ge et al. 2007). The interactions as well as the inhibitory effects of bismuth to fumarase have been characterized in this study. The titration of bismuth by fluorescence quenching experiments indicated that each fumarase monomer binds one mol equiv of Bi^{3+}. The secondary structural change during bismuth binding was negligible. Bismuth-binding results in a near stoichiometric inactivation of the enzyme. Our collective data may indicate that the TCA cycle is a potential molecular target of bismuth drugs in *H. pylori*, which will provide some clues for the future development of specific enzyme-targeting prodrugs.

Materials and methods

Materials

Chemicals were of the highest reagent grade commercially available and used without further purification. Stock solutions were prepared by dissolving anhydrous salts in Milli-Q (Millipore) purified water (18.2 MΩ) and adjusted to desired pH values with 1.0 M NaOH or HCl whenever needed. *L*-Malic acid and 5,5′-dithiobis(2-nitrobenzoicacid) (DTNB) were purchased from sigma.

Expression and purification of fumarase

The 1,392-bp gene of *H. pylori* fumarase was amplified by using the sense primer 5′-GGATTCA/TATGCAATTTAGAATTGAACATGAC-3′ and the antisense primer 5′-CACCC/TCGAGTTCCAGCCTTAGGCCCGAT-3′. The gene was inserted into the prokaryotic vector pET32a(+) and the recombinant plasmid (pET-fumarase) was validated by restriction enzyme analysis and sequencing. The *E. coli* BL21 (DE3) harboring the recombinant plasmid was cultured overnight in 2× YT medium supplemented with 100 μg/ml ampicillin and then diluted 1:100 into the Luria–Bertani medium containing 100 μg/ml ampicillin. When the OD_{600} value reached ~0.8, IPTG (0.1 mM) was added to induce the protein expression and cells were maintained at 37°C for another 4 h. The cells were collected by centrifugation at 5,000*g* for 30 min at 4°C, washed twice with phosphate-buffered saline (PBS), and then resuspended into buffer A (20 mM phosphate buffer, pH 7.4, 500 mM NaCl, 10 mM imidazole and 1% Triton X-100). The mixture was subjected to freezing-thawing thrice and ultrasonication. The lysates were

centrifuged at 16,000*g* for 15 min. The supernatant was filtered through a 0.45-μm-pore-size cellulose acetate syringe filter before loading onto a $NiSO_4$-impregnated HiTrap Chelating HP column (5 ml). Fumarase was eluted by buffer B (20 mM phosphate buffer, pH 7.4, 500 mM NaCl and 50 mM imidazole). Proteins were desalted into an appropriate buffer with a PD-10 column (GE Biosciences) (Ge et al. 2006a, b). The free thiolate content of fumarase was determined by Ellman's method as described previously (Ellman 1959; Jin et al. 2004). Fumarase was added into a 1 mM DTNB solution in 20 mM Hepes (pH 7.4) plus 100 mM NaCl to a final concentration of 2 μM. The amount of generated *p*-nitrothiolate was determined with the extinction coefficient (ε_{412}) of 13600 M^{-1} cm^{-1} (Ellman 1959). The purified proteins were subjected to mass spectrometric analysis. The protein bands were trypsin-digested overnight and analyzed with a 4800-plus matrix-assisted laser desorption/ionization time-of-flight/time-of-flight mass spectrometer (MS) (Applied Biosystems) (He et al. 2003; Ge et al. 2007; Sun et al. 2009). Peptide-mass fingerprinting was carried out with ProteinProspector program (Clauser et al. 1999) against the NCBI *H. pylori* 26695 database.

Gel electrophoresis

Sodium dodecyl sulfate–polyacrylamide gel electrophoresis (SDS–PAGE) was performed according to the method of Maniatis et al. (1982), and proteins were visualized with Coomassie Blue R-250. The aggregation state of recombinant fumarase proteins was also analyzed by non-denaturing polyacrylamide gel electrophoresis, according to the method of Coligan et al. (2001), calibrated with high molecular weight native markers (GE Biosciences).

Fast protein liquid chromatography

Fumarase was separated by fast protein liquid chromatography (FPLC; GE Biosciences) with a gel filtration Superdex 75 10/300 GL column, using running buffers containing 20 mM Tris–HCl, pH 7.6 and 100 mM NaCl. The column was calibrated with gel filtration HMW calibration kit (GE Biosciences): ovalbumin, 43 kDa; conalbumin, 75 kDa; aldolase, 158 kDa; ferritin, 440 kDa and thyroglobulin, 669 kDa. Blue dextrin was used to determine the void volume.

Fumarase enzymatic assay

Fumarase enzymatic activity was assayed at 25°C by monitoring the production of fumarate at 240 nm as previously described (Bergmeyer et al. 1974). The enzyme was incubated in 100 mM potassium phosphate buffer (pH 7.6) for 5 min at 25°C. Reaction was started by the addition of *L*-malic acid to a final concentration of 50 mM, and the absorbance at 240 nm was monitored as a function of time. Activities were expressed as μmol products formed per min at pH 7.6 and 25°C and were calculated using the molar coefficient of 2.44 × 10^3 M^{-1} cm^{-1} for fumarate. For inhibitory effects of bismuth on the fumarase activity, 1 and 1.5 mol equiv of $Bi(NO_3)_3$ were added into 80 nM fumarase solution containing a series of concentrations (5–15 mM) of *L*-malic acid. The K_m and V_{max} for uninhibited and inhibited reactions were obtained from Lineweaver–Burk plots:

$$1/V_0 = K_m/(V_{max}[S]) + 1/V_{max}.$$

Fluorescence changes during bismuth titration

Bismuth titration was performed on a Shimadzu RF-5301pc luminescence spectrometer. The excitation wavelength was set at 295 nm and the emission spectra were obtained at 300–450 nm. A solution of 0.5 μM fumarase was titrated with a series of concentrations of Bi^{3+} in 20 mM Tris–HCl (pH 7.5) plus 100 mM NaCl. Fluorescence emission intensities were corrected for dilution.

CD spectroscopy

CD spectra were determined on a Jasco J-810 spectropolarimeter pre-calibrated with a 0.06% (+)-10-camphorsulphonic acid solution (Sigma), using a 0.1-cm-pathlength quartz cell. CD data were obtained for 5 μM fumarase in PBS buffer, pH 7.5 in both the absence and the presence of 1 mol equiv of Bi^{3+}. Instrumental settings basically followed the method described previously (Ge et al. 2006a, b). Quantitative estimations of the secondary structural contents were

made using the CDPro software package (Sreerama and Woody 2000; Ge et al. 2006a, b; Sun et al. 2010).

Protein structure modeling

The structure of fumarase was modeled using the Swiss-Model Server (http://swissmodel.expasy.org/) (Arnold et al. 2006) based on the PDB structure of *E. coli* fumarase C (PDB entry 1fuo) (Weaver and Banaszak 1996). The modeled structure was visualized and analyzed with Pymol (DeLano 2008).

Results

Protein expression and purification

The fumarase gene (HP1325) was PCR amplified from the genomic DNA of *H. pylori* 26695. The gene was inserted into pET32a using the *Nde*I and *Xho*I restriction sites and verified by sequencing. The recombinant plasmid was transformed into *E. coli* BL21(DH3) and expression was induced with 0.1 mM IPTG when the OD_{600} reached around 0.8. The culture was further incubated for another 4–5 h at 37°C. It was found that the protein can bind with the nickel-charged iminodiacetate-derivatized agarose (HiTrap) without the fusion hexa-His tag in mild affinities. Comparably pure proteins were eluted with 50 mM imidazole. The fumarase protein has a calculated molecular weight of 50.9 kDa and p*I* of 6.79. By SDS–PAGE, the purified proteins appeared as two very close bands at around 45/43 kDa (Fig. 1). Both bands were verified to be fumarase through MS analysis (data not shown). The native state of the protein in the absence or in the presence of 1 mol equiv of Bi^{3+} was estimated by gel-filtration chromatography and non-denaturing PAGE. As shown in the elution profile for the apo-fumarase (Fig. 1), two fractions were present at approx. 7.8 and 8.5 ml respectively. Basically, the elution profile for one mol equiv of Bi^{3+}-loaded fumarase is quite similar to the apo-form, indicating that bismuth-binding has little effect on the oligomerization state of fumarase. On the non-denaturing PAGE, fumarase migrated as three bands, at approx. 230, 440 and 660 kDa when compared with the HMW calibration kit for native electrophoresis (GE Biosciences), corresponding to fumarase tetramer, octamer and dodecamer, respectively. As the tetramer is the functional group for class II fumarase enzymes (Weaver et al. 1995; Weaver and Banaszak 1996), the three bands on the non-denaturing PAGE could be regarded as the monomer, dimer and trimer of tetramer, respectively. It seems that there is an inconsistency between the gel filtration and non-denaturing PAGE experiments: 2 vs. 3 protein bands. This could be explained by the incapability of the gel filtration column to separate the two oligomers (~440 and 660 kDa, respectively), both of which were eluted in the void volume of the column (~7.8 ml in the elution profile as shown in Fig. 1).

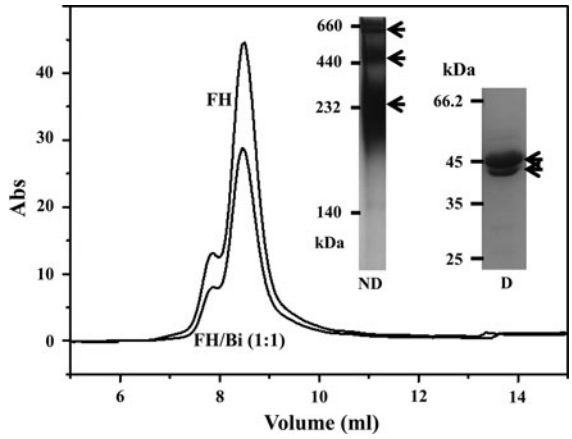

Fig. 1 Analysis of the fumarase by FPLC, denaturing and non-denaturing electrophoresis. Gel filtration profiles for fumarase and bismuth-bound fumarase on a Superdex 75 10/300GL column eluted with a buffer containing 20 mM Tris–HCl and 100 mM NaCl, pH 7.6, at room temperature. Three bands appeared on the non-denaturing electrophoresis gel, whereas on the SDS–PAGE, the purified proteins migrated as two very close bands at around 45/43 kDa. *Arrow* the protein band corresponding to the fumarase protein. Fumarase is abbreviated as FH in the figures

Inhibition study

The measured rates of *L*-malic acid dehydration catalyzed by fumarase at different concentrations were shown as Lineweaver–Burk plot in Fig. 2. The uninhibited reaction has a calculated K_m and V_{max} of 15.3 mM and 3.85 min^{-1}, respectively. The apparent V_{max} and K_m values changed to 1.43 and 0.56 min^{-1}, 11.56 and 10.29 mM respectively, upon the addition of 1 and 1.5 mol equiv of Bi^{3+}. The Lineweaver–Burk plots displayed an apparent non-competitive

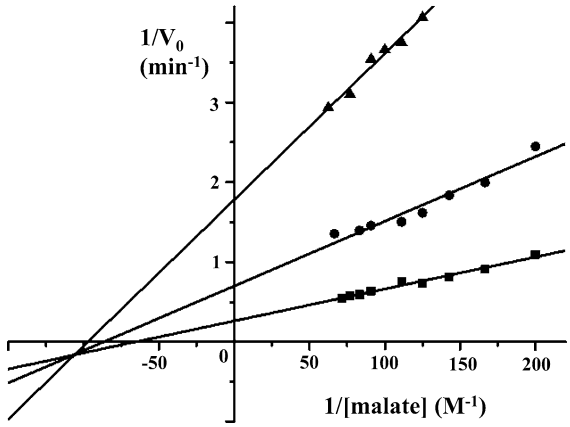

Fig. 2 Lineweaver–Burk plots of the dehydration of *L*-malic acid catalyzed by fumarase. The assay reaction is composed of 80 nM fumarase in 100 mM potassium phosphate buffer (pH 7.6) containing a series of concentrations (5–15 mM) of *L*-malic acid in the absence or in the presence of 1 and 1.5 mol equiv of $Bi(NO_3)_3$. Bi^{3+} concentrations were: *squares* none; *circles* 80 nM; *triangles* 160 nM. Each point is the mean of three determinations. The results show a non-competitive inhibition

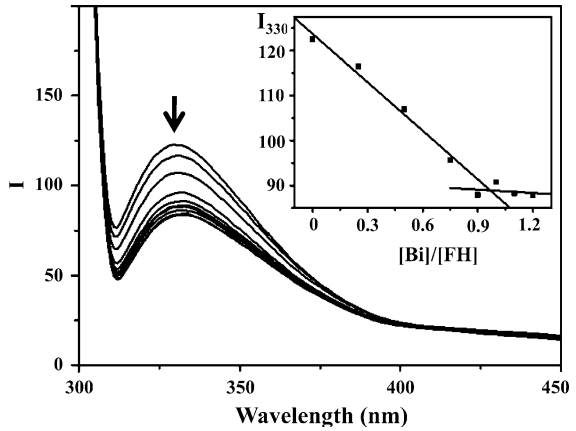

Fig. 3 Fluorescence spectra for the titration of bismuth ion into fumarase. *Insert* titration curve extracted at 330 nm

mechanism of enzyme inhibition. As per the standard approach, the apparent inhibition constant, K_i, was determined to be 47.3 and 20.4 nM in the presence of 1 and 1.5 equivalents of bismuth, respectively. The K_i values are too wide to guarantee the following of the normal way of non-competitive mechanism of enzyme inhibition by bismuth. The actual mechanism may be quite complicated and the pattern is likely to arise from inactivation of a portion of the enzyme with the remaining activity appearing to have decreased V_{max} and the same K_m. The data are most compatible with one equivalent inactivating 63% of the sample (V_{max} is reduced from 3.85 to 1.43 min^{-1}) and 1.5 equivalents inactivating 86% of the sample (V_{max} is reduced to 0.56 min^{-1}).

Fluorescence changes during bismuth titration

Fluorescence changes were followed during bismuth titration into fumarase. There are two tryptophan residues and three tyrosine residues in each subunit of fumarase, which contribute to the intrinsic fluorescence at 330 nm. The fluorescence emission intensity significantly decreased upon the addition of bismuth(III) (Fig. 3). This suggested that conformational changes occurred upon bismuth(III) binding. The fluorescence at 330 nm with the titration of bismuth in the insert showed that each fumarase monomer binds one mol equiv of Bi^{3+}.

Structural characterizations of fumarase upon bismuth-binding

To further investigate the effect of bismuth binding on the secondary structure of fumarase, CD spectra were collected at room temperature. The CD spectrum of apo-fumarase in 20 mM Tris–HCl at pH 7.4 is characterized by two negative peaks at 210 and 220 nm and a positive peak at around 196 nm (Fig. 4A), a feature of the overwhelming presence of α-helix and residual presence of β-sheet, turn and unordered forms. Quantitative analysis with CDPro (Sreerama and Woody 2000) confirmed that fumarase is almost exclusively present as right-handed α-helix. The CD spectrum of the bismuth-binding form of fumarase (Bi:fumarase 1:1) is roughly similar with the apo-protein. The CDPro quantization indicated that 80.2% right-handed and 19.8% left-handed α-helix are present in the holo-protein solution. The chiral overturn of part of the fumarase α-helices upon bismuth binding seemed to indicate the reorganization of the local environment around the bismuth-binding site. This may represent the incorrect interpretation of the CD data by CDPro software, as left-handed α-helix (Novotny and Kleywegt 2005) exist exclusively in peptides containing D-amino acids (Anil et al. 2004) and in poly-Gly strands (Hovmoller et al. 2002), which is not the case for

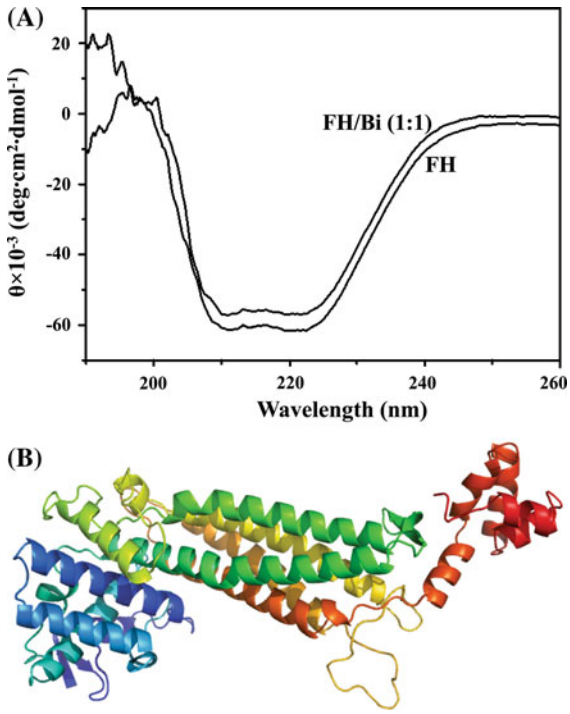

Fig. 4 Structural characterizations of fumarase. **a** Circular dichroism spectra of the apo- and bismuth-loaded fumarase CD data were obtained for 5 μM fumarase in PBS buffer, pH 7.5 in both the absence and the presence of 1 mol equiv of Bi^{3+}. **b** Homology modeling of fumarase

fumarase. On the basis of the crystal structure of *E. coli* fumarase C and sequence homology alignment, the fumarase structure was simulated and the modeled structure consists of 455 amino acids (residues 4–458) in three domains (Fig. 4B). The central domain is composed of a five-helix bundle, the association of which is responsible for the tetramer formation in *E. coli* homologue (Weaver et al. 1995). The other two domains clip the helical bundle on the opposite ends to give a dumbbell-like structure. As determined from the CD experiments, helix is dominant in the modeled fumarase structure.

Thiolate group analysis of fumarase

In order to investigate whether Bi^{3+} binds to free cysteine residues of fumarase, free thiolate contents were determined by DTNB. In total there are six cysteine residues in the amino acid sequence of fumarase. The native enzyme was determined to have three free thiolate groups. After incubation with 1 mol equiv of Bi^{3+} at 25°C for 3 h, the number of free thiolate groups decreased to 2, indicating the involvement of cysteine in bismuth binding.

Discussion

H. pylori infects around half of the world's population and causes various gastric diseases. Bismuth-based triple therapy has been commonly recommended for eradicating *H. pylori* (Xia et al. 2002). Up to now, the molecular mechanisms underlying the antimicrobial activities of bismuth remain to be fully established, albeit several possible mechanisms have been proposed: inhibition of proteases (Ge et al. 2007), urease (Zhang et al. 2006), and alcohol dehydrogenase (Jin et al. 2004); modulation of cellular oxidative stress; interference with nickel homeostasis (Ge and Sun 2007; Ge et al. 2007); inhibition of protein and cell wall synthesis, membrane function and ATP synthesis (Lambert and Midolo 1997). Our previous proteomic work observed that the level of at least four proteins, one elongation factor Ef-Tu, fumarase, two established metal-binding proteins HspA (Cun et al. 2008) and NapA (Dundon et al. 2001; Sun et al. 2008), dramatically decreased upon Bi-IMAC enrichment from bismuth-treated cell extracts as compared to untreated cells. The results suggested that these four proteins may be the chief targeting sites of bismuth in vivo.

Fumarase is a key enzyme in the TCA cycle and in amino acid metabolism to catalyze the reversible and stereo-specific hydration/dehydration of fumarate to *L*-malic acid. Fumarase can be classified into class I and II based on its oligomerization state and metal cofactor requirements (Guest et al. 1985; Woods et al. 1988): class I, iron-dependent, dimer; class II, no known metal ion requirement, tetramer. Only one fumarase gene is present in the genome of *H. pylori* 26695 and is designated as class II fumarase based on sequence homology (Tomb et al. 1997). In this present study, the fumarase gene was cloned and recombinantly expressed in *E. coli* without any tag with acceptable purity to preserve it native state. On non-denaturing PAGE, three bands appeared and were determined to be tetramer, octamer and dodecamer. As the tetramer is the basic functional group (Weaver et al. 1995; Weaver and Banaszak 1996), it is supposed to be the monomer, dimer and trimer of

tetramer, respectively. Purified fumarase proteins migrated with two close bands of 45 and 43 kDa on SDS–PAGE. Both bands were identified as fumarase through MS analysis. The doublet bands were probably due to a partial C-terminal cleavage (Celerier et al. 2000), phosphorylation (van Veen et al. 2000), or some degradation reasons (Arcucci et al. 2006). The detailed reason is unknown for now and deserves further efforts in this regards. However fumarase was identified as a series of parallel isoforms (similar molecular weight and differential p*I* values) in our previous 2D gel-based work (Ge et al. 2007), suggesting that phosphorylation may play roles in the isoform formation.

The extensive fluorescence quenching upon bismuth binding may result from the local environmental changes around one or even more of the three tryptophans present in the amino acid sequence of fumarase, in which the energy transfer may occur between tryptophan(s) and other aromatic groups that are brought nearby owing to the conformational change induced by bismuth binding. According to the modeled structure of fumarase, one of the three tryptophans, W-295 is localized on one tail of the central five-helix bundle domain; whereas the other three tryptophans, W-21 and W-93 are present on the loops of the same "cap" domain, on the far side of W-295. Two active sites, A-site and B-site, are present in the two "cap" domains on the functional fumarase tetramer (Weaver et al. 1995; Weaver and Banaszak 1996). As the five-helix bundle domain is comparably rigid, the "loop" tryptophans, W-21 and W-93, may be more accessible to structural change and are responsible for the identified fluorescence quenching upon bismuth binding. Our ongoing crystallographic analysis of the fumarase structure, especially the bismuth-bound holo form, may be able to confirm this speculation.

Bismuth-binding results in a near stoichiometric inactivation of the enzyme, despite the fact that a non-competitive mechanism was apparent from the Lineweaver–Burk plots. Yogev et al. found that cytosolic fumarase is involved in recognition and recovery from DNA damage, mainly from DNA double-strand breaks (Yogev et al. 2010). Therefore fumarase is a critical factor for many cellular processes. The inhibition of this enzyme by bismuth is thus a molecular mechanism underlying the inhibitory effects of bismuth-based drugs against *H. pylori*.

Acknowledgments The authors thank the anonymous reviewer for insightful comments. This work was supported by National Natural Science Foundation of China (20801061), Guangdong Natural Science Foundation (8451027501001233) and the Fundamental Research Funds for the Central Universities (10lgpy19).

References

Anil B, Song B, Tang Y, Raleigh DP (2004) Exploiting the right side of the Ramachandran plot: substitution of glycines by D-alanine can significantly increase protein stability. J Am Chem Soc 126:13194–13195

Arcucci A, Montagnani S, Gionti E (2006) Expression and intracellular localization of Pyk2 in normal and v-src transformed chicken epiphyseal chondrocytes. Biochimie 88:77–84

Arnold K, Bordoli L, Kopp J (2006) The SWISS-MODEL workspace: a web-based environment for protein structure homology modelling. Bioinformatics 22:195–201

Bergmeyer HU, Gawehn K, Grassl M (1974) In: HU Bergmeyer (ed) Methods of enzymatic analysis. Academic Press, New York

Blaser MJ (1987) Gastric *Campylobacter*-like organisms, gastritis, and peptic ulcer disease. Gastroenterology 93:371–383

Celerier J, Schmid G, Le Caer JP, Gimenez-Roqueplo AP, Bur D, Friedlein A, Langen H, Corvol P, Jeunemaitre X (2000) Characterization of a human angiotensinogen cleaved in its reactive center loop by a proteolytic activity from Chinese hamster ovary cells. J Biol Chem 275:10648–10654

Clauser KR, Baker P, Burlingame AL (1999) Role of accurate mass measurement (±10 ppm) in protein identification strategies employing MS or MS/MS and database searching. Anal Chem 71:2871–2882

Coligan JE, Dunn BM, Ploegh HL, Speicher DW, Wingfield PT (2001) Current protocols in protein science. Wiley, New York

Cun S, Li H, Ge R, Lin MC, Sun H (2008) A histidine-rich and cysteine-rich metal-binding domain at the C terminus of heat shock protein A from *Helicobacter pylori*: implication for nickel homeostasis and bismuth susceptibility. J Biol Chem 283:15142–15151

DeLano WL (2008) The PyMOL molecular graphics system. DeLano Scientific LLC, Palo Alto

Dundon WG, Polenghi A, Del Guidice G, Rappuoli R, Montecucco C (2001) Neutrophil-activating protein (HP-NAP) versus ferritin (Pfr): comparison of synthesis in *Helicobacter pylori*. FEMS Microbiol Lett 199:143–149

Ellman GL (1959) Tissue sulfhydryl groups. Arch Biochem Biophys 82:70–77

Ge Z (2002) Potential of fumarate reductase as a novel therapeutic target in *Helicobacter pylori* infection. Expert Opin Ther Targets 6:135–146

Ge R, Sun H (2007) Bioinorganic chemistry of bismuth and antimony: target sites of metallodrugs. Acc Chem Res 40:267–274

Ge Z, Feng Y, Dangler CA, Xu S, Taylor NS, Fox JG (2000) Fumarate reductase is essential for *Helicobacter pylori*

colonization of the mouse stomach. Microb Pathog 29:279–287

Ge R, Watt RM, Sun X, Tanner JA, He QY, Huang JD, Sun H (2006a) Expression and characterization of a histidine-rich protein, Hpn: potential for Ni^{2+} storage in *Helicobacter pylori*. Biochem J 393:285–293

Ge R, Zhang Y, Sun X, Watt RM, He QY, Huang JD, Wilcox DE, Sun H (2006b) Thermodynamic and kinetic aspects of metal binding to the histidine-rich protein, Hpn. J Am Chem Soc 128:11330–11331

Ge R, Sun X, Gu Q, Watt RM, Tanner JA, Wong BC, Xia HH, Huang JD, He QY, Sun H (2007) A proteomic approach for the identification of bismuth-binding proteins in *Helicobacter pylori*. J Biol Inorg Chem 12:831–842

Guest JR, Miles JS, Roberts RE, Woods SA (1985) The fumarase genes of *Escherichia coli*: location of the fumB gene and discovery of a new gene (fumC). J Gen Microbiol 131:2971–2984

He QY, Lau GK, Zhou Y, Yuen ST, Lin MC, Kung HF, Chiu JF (2003) Serum biomarkers of hepatitis B virus infected liver inflammation: a proteomic study. Proteomics 3:666–674

Hovmoller S, Zhou T, Ohlson T (2002) Conformations of amino acids in proteins. Acta Crystallogr D 58:768–776

Jin L, Szeto KY, Zhang L, Du W, Sun H (2004) Inhibition of alcohol dehydrogenase by bismuth. J Inorg Biochem 98:1331–1337

Lambert JR, Midolo P (1997) The actions of bismuth in the treatment of *Helicobacter pylori* infection. Aliment Pharmacol Ther 11:27–33

Maniatis T, Fritsch EF, Sambrook J (1982) Molecular cloning: a laboratory manual. Cold Spring Harbor Laboratory Press, New York

Megraud F (2004) Basis for the management of drug-resistant *Helicobacter pylori* infection. Drugs 64:1893–1904

Mendz GL, Hazell SL, Srinivasan S (1995) Fumarate reductase: a target for therapeutic intervention against *Helicobacter pylori*. Arch Biochem Biophys 321:153–159

Novotny M, Kleywegt GJ (2005) A survey of left-handed helices in protein structures. J Mol Biol 347:231–241

Pitson SM, Mendz GL, Srinivasan S, Hazell SL (1999) The tricarboxylic acid cycle of *Helicobacter pylori*. Eur J Biochem 260:258–267

Sreerama N, Woody RW (2000) Estimation of protein secondary structure from circular dichroism spectra: comparison of CONTIN, SELCON, and CDSSTR methods with an expanded reference set. Anal Biochem 287:252–260

Sudarshan S, Linehan WM, Neckers L (2007) HIF and fumarate hydratase in renal cancer. Br J Cancer 96:403–407

Sun H, Szeto KY (2003) Binding of bismuth to serum proteins: implication for targets of Bi(III) in blood plasma. J Inorg Biochem 94:114–120

Sun H, Li H, Harvey I, Sadler PJ (1999) Interactions of bismuth complexes with metallothionein(II). J Biol Chem 274:29094–29101

Sun X, Ge R, Chiu JF, Sun H, He QY (2008) Identification of proteins related to nickel homeostasis in *Helicobacter pylori* by immobilized metal affinity chromatography and two-dimensional gel electrophoresis. Met Based Drugs 2008:289490

Sun X, Ge R, Cai Z, Sun H, He Q-Y (2009) Iron depletion decreases proliferation and induces apoptosis in a human colonic adenocarcinoma cell line, $Caco_2$. J Inorg Biochem 103:1074–1081

Sun X, Ge R, Zhang D, Sun H, He QY (2010) Iron-containing lipoprotein SiaA in SiaABC, the primary heme transporter of *Streptococcus pyogenes*. J Biol Inorg Chem 15:1265–1273

Tomb JF, White O, Kerlavage AR, Clayton RA, Sutton GG, Fleischmann RD, Ketchum KA, Klenk HP, Gill S, Dougherty BA, Nelson K, Quackenbush J, Zhou L, Kirkness EF, Peterson S, Loftus B, Richardson D, Dodson R, Khalak HG, Glodek A, McKenney K, Fitzegerald LM, Lee N, Adams MD, Hickey EK, Berg DE, Gocayne JD, Utterback TR, Peterson JD, Kelley JM, Cotton MD, Weidman JM, Fujii C, Bowman C, Watthey L, Wallin E, Hayes WS, Borodovsky M, Karp PD, Smith HO, Fraser CM, Venter JC (1997) The complete genome sequence of the gastric pathogen *Helicobacter pylori*. Nature 388:539–547

van Veen TA, van Rijen HV, Jongsma HJ (2000) Electrical conductance of mouse connexin45 gap junction channels is modulated by phosphorylation. Cardiovasc Res 46:496–510

Weaver T, Banaszak L (1996) Crystallographic studies of the catalytic and a second site in fumarase C from *Escherichia coli*. Biochemistry 35:13955–13965

Weaver TM, Levitt DG, Donnelly MI, Stevens PP, Banaszak LJ (1995) The multisubunit active site of fumarase C from *Escherichia coli*. Nat Struct Biol 2:654–662

Woods SA, Schwartzbach SD, Guest JR (1988) Two biochemically distinct classes of fumarase in *Escherichia coli*. Biochim Biophys Acta 954:14–26

Xia HH, Wong BC, Talley NJ, Lam SK (2002) Alternative and rescue treatment regimens for *Helicobacter pylori* eradication. Expert Opin Pharmacother 3:1301–1311

Yang Y, Valera VA, Padilla-Nash HM, Sourbier C, Vocke CD, Vira MA, Abu-Asab MS, Bratslavsky G, Tsokos M, Merino MJ, Pinto PA, Srinivasan R, Ried T, Neckers L, Linehan WM (2010) UOK 262 cell line, fumarate hydratase deficient (FH−/FH−) hereditary leiomyomatosis renal cell carcinoma: in vitro and in vivo model of an aberrant energy metabolic pathway in human cancer. Cancer Genet Cytogenet 196:45–55

Yogev O, Singer E, Shaulian E, Goldberg M, Fox TD, Pines O (2010) Fumarase: a mitochondrial metabolic enzyme and a cytosolic/nuclear component of the DNA damage response. PLoS Biol 8:e1000328

Zhang L, Mulrooney SB, Leung FK, Zeng YB, Ko BBC, Hausinger RP, Sun H (2006) Inhibition of urease by bismuth(III): implications for the mechanisms of action of bismuth drugs. Biometals 19:503–511